INTERNATIONAL JOURNAL FOR NUMERICAL METHODS IN FLUIDS
Int. J. Numer. Meth. Fluids 2002; **40**:1075–1081 (DOI: 10.1002/fld.393)

Parallel computations of natural convection flow in a tall cavity using an explicit finite element method

Timothy A. Dunn*,† and Rose C. McCallen

Lawrence Livermore National Laboratory, Livermore, CA 94550, U.S.A.

SUMMARY

An explicit finite element method was used to predict a natural convection flow in an enclosed cavity. The problem considered was a differentially heated, tall (8:1), rectangular cavity with a Rayleigh number of 3.4×10^5 and Prandtl number of 0.71. The incompressible Navier–Stokes equations were solved using a Boussinesq approximation for the buoyancy force. The algorithm was developed for efficient use on massively parallel computer systems with emphasis on time-accurate simulations. It was found that the average temperature and velocity values can be captured with a relatively coarse grid, while the oscillation amplitude and period appear to be grid sensitive and require a refined computation. Copyright © 2002 John Wiley & Sons, Ltd.

KEY WORDS: incompressible flow; natural convection; Boussinesq; Navier–Stokes; finite element method; cavity

1. INTRODUCTION

Thermal convection is an important phenomena in a variety of practical engineering applications. These flows can exhibit highly three-dimensional, unsteady behaviour around complex geometries and involve a wide range of length scales. Therefore, simulations of these types of problems require time-accurate computations with very fine spatial resolution. Conventional, serial simulations on large grids are too computationally expensive for many flows of interest. Therefore, parallel computations are required for reasonable execution times.

Before large, complex simulations can be performed, it is essential to validate the performance of the computational tools on smaller test cases with established solutions. That was the motivation for the current investigation. The focus of this test was the 8:1 differentially heated cavity with a Rayleigh number (Ra) of 3.4×10^5 and a Prandtl number (Pr) of 0.71. Although geometrically 'simple', this benchmark problem exhibits many of the complex flow features associated with many problems of interest. In particular, the defined flow has unsteady, yet

* Correspondence to: T. A. Dunn, Lawrence Livermore National Laboratory, Livermore, CA 94550, U.S.A.
† E-mail: dunn13@llnl.gov.

Contract/grant sponsor: U.S. Department of Energy; contract/grant number: W-7405-Eng-48

Received 31 December 2001
Revised 1 July 2002

periodic, flow within the 'critical' regime where transition from steady to turbulent flow is initiated. The guidelines outlined in Reference [1] for the problem's initial/boundary conditions were followed in setting up and generating the following results.

2. METHODOLOGY

An Eulerian formulation of the time-dependent three-dimensional incompressible Navier–Stokes equations was solved using the Galerkin finite element method (FEM). This method is described in detail in Reference [2]. The discretized continuity and momentum equations can be written in matrix form as

$$\mathbf{C}^{\mathrm{T}}u = 0 \tag{1}$$

$$\mathbf{M}\dot{u} + (\mathbf{K} + \mathbf{N}(u))u + \mathbf{C}P = f \tag{2}$$

where u is the velocity vector and P is the pressure divided by density. $\mathbf{M}$, $\mathbf{K}$, and $\mathbf{N}(u)$ are the mass, diffusion, and advection matrices, respectively. The matrix $\mathbf{C}$ is the gradient operator and its transpose is the divergence operator. The force vector, f, incorporates the Boussinesq approximation to the buoyancy term and is integrated over the volume resulting in

$$f = \vec{g}(1 - \beta(T - T_0))\Omega_{\mathrm{e}} \tag{3}$$

where $\vec{g}$ is the gravitational acceleration, β is the coefficient of thermal expansion, T_0 is a reference temperature, T is the temperature and Ω_{e} is the element volume.

In the current implementation, the Q1Q0 element formulation was used for eight-node hexahedral brick elements. This provides linear velocity interpolation and piecewise constant pressure. Note that the above element is three dimensional while the problem of interest is two dimensional. Therefore, a single element was used in the out-of-plane direction and the out-of-plane velocity was set to zero.

The coefficient matrices were generated using one-point Gaussian quadrature. Therefore, hourglass correction was added to the diffusion matrix to damp any zero-energy modes that may be present because of the reduced integration scheme [3]. Computations with full (eight-point) quadrature, which do not require hourglass correction, were also performed, but no noticeable differences in the results were found. Balancing tensor diffusivity was added to balance the negative diffusion induced by the explicit Euler time integration. To reduce the computational effort, a 'centroid advection velocity' approximation was used in the evaluation of the advection term.

The continuity and momentum equations were solved simultaneously for the velocity and pressure with an explicit forward-Euler time integration

$$\begin{bmatrix} \mathbf{M}_{\mathbf{L}} & \mathbf{C} \\ \mathbf{C}^{\mathrm{T}} & \mathbf{0} \end{bmatrix} \begin{bmatrix} \dfrac{u^{n+1}}{\Delta t} \\ P^n \end{bmatrix} = \begin{bmatrix} F \\ 0 \end{bmatrix} \tag{4}$$

where $F = f^n + ((1/\Delta t)\mathbf{M}_{\mathbf{L}} - \mathbf{K} - \mathbf{N}(u^n))u^n$, Δt is the time step, and n is the current time-step level. A row-sum lumped mass approximation was used for the mass matrix (indicated by the subscript $\mathbf{L}$) for improved efficiency during the matrix solve.

The above system of equations was assembled using the finite element interface [4] and solved using the HYPRE parallel solver package [5]. The above library packages provide many advanced iterative linear solvers and preconditioners designed for efficient matrix solutions on massively parallel computer systems. In particular, the solver uncouples the pressure from the velocity by forming the Schur compliment of Equation (4) resulting in an equivalent pressure Poisson equation (PPE) which was solved for pressure. The pressure was then back substituted into the original matrix to solve for the velocity. For all results presented here, the PPE was solved using the conjugate gradient solver with parallel sparse approximate inverse (ParaSails) preconditioning.

The temperature was solved independent of the flow equations. The advection–diffusion equation is used for thermal transport and can be expressed in matrix form as

$$\mathbf{M}_{\mathrm{ad}}\dot{T} + (\mathbf{K}_{\mathrm{ad}} + \mathbf{N}_{\mathrm{ad}}(u))T = f_{\mathrm{ad}} \tag{5}$$

where T is the temperature. The subscript ad is used to differentiate between the similar matrices and source terms found in the momentum equation (see Reference [2] for matrix definitions). This equation was solved with the Galerkin FEM using tri-linear basis functions for the temperature and second-order Gaussian quadrature for the spatial integration. An explicit time-integration scheme with a lumped-mass approximation was used so that no matrix solve was required. A stable explicit solution of the thermal equations required a time step that was approximately half the size of the time steps required for the flow. Therefore, thermal sub-cycling was utilized, such that two thermal steps were taken for each solution of the flow equations. The temperature was fed back into the momentum equation via Equation (3).

3. RESULTS

The results presented here were based on the guidelines outlined in Reference [1], which defines the non-dimensional values and nomenclature used below. Although other cases were investigated, only results for the specified $Ra = 3.4 \times 10^5$ and $Pr = 0.71$ are reported here.

The solution was calculated on three grids: 30×100, 60×200, and 90×300 elements. The grid spacing was graded with a 3:1 ratio from the centre of the cavity to the wall. The simulations produced unsteady, time-periodic solutions on all three grids. The fluctuations are characterized by small 'pockets' of hot and cold fluid. Figure 1 shows these perturbations at several snapshots during a single period. Here the perturbation temperature was calculated by subtracting the mean temperature value from the instantaneous value. As the time progressed, these pockets advected along with the flow, travelling up the hot wall on the left and down the cold wall on the right. These pockets account for the oscillations in temperature observed at points throughout the cavity.

During the flow solution, time-history data at various points in the cavity (see Reference [1] for details) were reported at each time step. Time–history plots of the non-dimensional temperature at point 1 (θ_1) are found in Figure 2. All three simulations reveal an initial transient followed by a stationary state where the temperature exhibited periodic oscillations about a mean temperature value. These oscillations are clearly seen in the blow-up of the curve in the lower part of each graph.

Table I provides a summary of the time–history data for the three grid resolutions. The time-averaged value is given along with the amplitude and period of the oscillations for

Figure 1. Snapshots of instantaneous temperature perturbations over one time period $\mathcal{T}$. The dark regions represent temperatures greater than the mean and light (grey) regions represent temperatures less than the mean. These results were obtained with the 60×200 grid.

each variable presented in the table. The time average was integrated over 10 complete time periods ($10\mathcal{T}$) near the end of the calculation. The amplitude is defined as the peak-to-valley amplitude and was computed as the difference between the maximum and minimum value over the same time duration used to compute the average.

At point 1, the table presents information for the velocity in the x direction (u_1), the velocity in the y direction (v_1), the temperature (θ_1), and the vorticity (ω_1). The pressure differences ($\Delta P_{ij} = P_i - P_j$) are shown, where i and j indicate particular points in the cavity. Also presented are the Nusselt number (Nu) integrated along each vertical wall and the global metrics of kinetic energy ($\hat{u}$) and enstrophy ($\hat{\omega}$). It is observed that all of the grids gave similar answers for the average values, but very different results were obtained on the coarse grid for the amplitude and period. The amplitude of the temperature at point 1 increased 89% between the coarse and medium grids, while the same amplitude only changed by about 1% between the medium and fine grids. Similar comparisons were found with the amplitudes of the other quantities as well as the period of the oscillations. Therefore, further grid refinement is not expected to have significant effect on the reported values. It is believed that the differences observed in the coarse and medium grids were not only related to the spatial resolution, but also to the temporal resolution, since the coarse grid solution used a much larger time step than the solution on the medium grid. The period of oscillation for all of the variables was consistent for each simulation, indicating a single dominant frequency was present within the flow field. The skewness ($\varepsilon_{12} = \theta_1 + \theta_2$) was found to be very close to zero for all meshes, indicating a highly skew-symmetric temperature field.

The computations were performed in parallel on the IBM-based ASCI Blue-Pacific computer at LLNL. The machine is a distributed memory system with MPI used for message passing. The three grids used 4, 12 and 28 processors, respectively. The number of processors was

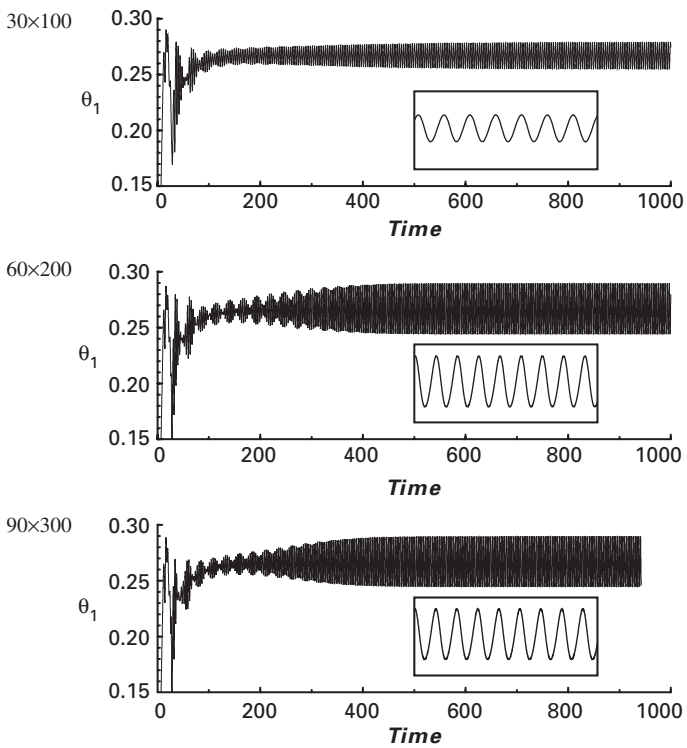

Figure 2. Temperature–time history at point 1 for the three grids. The blow-up window in each plot reveals the stable oscillatory solution obtained at time ≈900.

chosen such that fewer than 1000 elements were computed on each domain. Although this utilized more processors than would generally be used for a problem of this size, an excessive number was chosen in order to exercise the parallel capability. The wall-clock time per element per cycle was 720 μs for the 30×100 grid, 370 μs for the 60×200 grid, and 245 μs for the 90×300 grid. Notice that as the problems size increases, the methods utilized in the linear algebra libraries became more efficient. However, due to the reduced grid spacing, the restrictions on the explicit time-step size still makes the large-grid computations very expensive.

4. CONCLUSIONS

Time-accurate solutions were computed for the 8:1 differentially heated cavity with a Rayleigh number of 3.4×10^5 and Prandtl number of 0.71. Periodic solutions were obtained on all three of the grid resolutions tested. A few conclusions are summarized here.

- Although it appears that the average value for the velocity and temperature data can be fairly accurately calculated using a coarse grid, the time-accurate statistics such as oscillation amplitude and frequency appear highly grid dependent.

Table I. Compulsory point, wall, and global data for the three grids.

	Grid: 30×100 $\Delta x_{\min}$: 0.01818 $\Delta y_{\min}$: 0.0439 Steps/period: 72			Grid: 60×200 $\Delta x_{\min}$: 0.00912 $\Delta y_{\min}$: 0.0220 Steps/period: 216			Grid: 90×300 $\Delta x_{\min}$: 0.00609 $\Delta y_{\min}$: 0.01464 Steps/period: 489		
Quantity	Avg	Amp	Per	Avg	Amp	Per	Avg	Amp	Per
Point data									
u_1	0.0565	0.0292	4.23	0.0575	0.0576	3.47	0.0572	0.0575	3.44
v_1	0.459	0.0475	4.23	0.462	0.0806	3.47	0.462	0.0803	3.44
θ_1	0.267	0.0241	4.23	0.265	0.0455	3.47	0.266	0.0450	3.44
ε_{12}	0.0	0.0	—	0.0	0.0	—	0.0	0.0	—
ω_1	−2.37	0.649	4.23	−2.48	0.995	3.47	−2.36	1.131	3.44
ΔP_{14}	−2.62e-3	0.01149	4.23	−2.24e-3	2.20e-2	3.47	−1.949e-3	0.0215	3.44
ΔP_{51}	−2.19	0.01173	4.23	−2.19	0.0245	3.47	−2.21	0.0234	3.44
ΔP_{35}	−1.180	2.62e-3	4.23	−1.163	0.01154	3.47	−1.159	0.01075	3.44
Wall data									
$Nu_{x=0}$	−4.55	3.69e-3	4.23	−4.57	7.67e-3	3.47	−4.58	7.53e-3	3.44
$Nu_{x=W}$	−4.55	3.69e-3	4.23	−4.57	7.67e-3	3.47	−4.58	7.53e-3	3.44
Global data									
$\hat{u}$	0.239	1.159e-4	4.23	0.240	5.15e-5	3.47	0.240	4.61e-5	3.44
$\hat{\omega}$	3.00	2.41e-3	4.23	3.01	3.28e-3	3.47	3.02	3.31e-3	3.44

- Despite the very small time steps used in the current simulations, it is believed that the first-order time-accuracy associated with the forward Euler time-stepping scheme influenced the solution. This may have contributed to the poor predictions of the period on the coarse grid, which used relatively large time steps. Therefore, it is possible that a higher order time-stepping algorithm could improve these predictions with little increase in computational cost.
- The solution is very sensitive to the details in the algorithm. Although not presented here, solutions were obtained, by solving Equation (4) for the acceleration rather than the velocity. Although mathematically equivalent, solution of the acceleration resulted in the amplitude of the fluctuations to be greatly reduced or damped out completely. This damping is believed to be caused by slight deviations from the divergence-free field due to truncation error.
- Although most of the attention in this paper (as well as others presented at the First MIT Conference [1]) was dedicated to the flow equations, the solutions were highly influenced by the algorithm used to solve the temperature. Therefore, additional study should be conducted on the thermal solve.

ACKNOWLEDGEMENTS

This work was performed under the auspices of the U.S. Department of Energy by the University of California, Lawrence Livermore National Laboratory under Contract No. W-7405-Eng-48.

REFERENCES

1. Christon MA, Gresho PM, Sutton SB. Computational predictability of natural convection flows in enclosures. *International Journal for Numerical Methods in Fluids* 2002; **40**:953–980.
2. Gresho PM, Chan ST, Lee RL, Upson CD. A modified finite element method for solving the time-dependent, incompressible Navier–Stokes equations part 1: theory. *International Journal for Numerical Methods in Fluids* 1984; **4**(6):557–598.
3. Goudreau GL, Hallquist JO. Recent developments in large-scale finite element Lagrangian hydrocode technology. *Computational Methods in Applied Mechanics and Engineering* 1982; **33**(1–3):725–757.
4. Clay RL, Mish KD, Otero IJ, Taylor LM, Williams AB. An annotated reference guide to the finite-element interface (FEI) specification version 1.0. *Technical Report SAND*99-8229, Sandia National Laboratories, Livermore, CA, January 1999.
5. Chow E, Cleary AJ, Falgout RD, Lambert M, Tong C, Walker D, Yang UM. HYPRE, high performance preconditioners: user's manual, v.1.2.0. *Technical Report UCRL-MA*-137155-DR, Lawrence Livermore National Laboratory, Livermore, CA, August 2000.

